(In)coherent multiproxy signals in marine sediments: Implications for high-resolution paleoclimate reconstruction

Author(s):
Ausín, Blanca; Magill, Clayton; Haghipour, Negar; Fernandez, Alvaro; Wacker, Lukas; Hodell, David; Baumann, Karl-Heinz; Eglinton, Timothy I.

Publication date:
2019-06-01

Permanent link:
https://doi.org/10.3929/ethz-b-000334985

Originally published in:
Earth and Planetary Science Letters 515, https://doi.org/10.1016/j.epsl.2019.03.003

Funding acknowledgement:
175823 - TEMPORAL RELATIONSHIPS AMONG PROXY SIGNALS IN MARINE SEDIMENTS (TRAMPOLINE) (SNF)

Earth and Planetary Science Letters 515 (2019) 38–46

Contents lists available at ScienceDirect

Earth and Planetary Science Letters

www.elsevier.com/locate/epsl

(In)coherent multiproxy signals in marine sediments: Implications for high-resolution paleoclimate reconstruction

Blanca Ausín [a,*], Clayton Magill [a,b], Negar Haghipour [a,c], Álvaro Fernández [a], Lukas Wacker [c], David Hodell [d], Karl-Heinz Baumann [e], Timothy I. Eglinton [a]

[a] Geological Institute, ETH Zürich, Sonneggstrasse 5, Zurich 8092, Switzerland
[b] Lyell Centre, Heriot-Watt University, Edinburgh, Currie EH14 4AS, United Kingdom
[c] Laboratory of Ion Beam Physics, ETHZ, Otto-Stern Weg 5, HPK, 8093 Zurich, Switzerland
[d] Department of Earth Sciences, University of Cambridge, Downing St, Cambridge CB2 3EQ, United Kingdom
[e] Department of Geosciences, University of Bremen, Klagenfurter Straße, Bremen 28359, Germany

ARTICLE INFO

Article history:
Received 20 August 2018
Received in revised form 26 December 2018
Accepted 3 March 2019
Available online xxxx
Editor: J. Adkins

Keywords:
radiocarbon chronostratigraphy
age offsets
proxy bias
Iberian margin
age structure

ABSTRACT

Accurate chronologies are the backbone of paleoclimate research, yet for marine sedimentary records the same age model is often applied to co-eval components that may have experienced different pre-depositional histories, leading to aliasing in corresponding proxy signals. Here we demonstrate ^{14}C age discrepancies among several proxy carriers and use them to highlight spatio-temporal disparities among different components of the sediment. Total organic carbon (TOC), alkenones, and alkanoic (fatty) acids have older ages than co-occurring planktonic foraminifera in corresponding depth intervals of a sediment core retrieved from the so-called 'Shackleton Sites' on the southwest Iberian margin off Portugal. Temporal differences are explained by the addition of pre-aged material that is transported to the site by lateral advection, rivers or wind. We then modeled the age structure and relative abundance of the different pools that might have contributed to the older ages of TOC and alkenones. Results suggest the addition of a moderate (15-20%) proportion of very old allochthonous material (18,500-49,900 yr). This information was used to deconvolve the alkenone-derived sea surface temperature (SST) record and assess the impact of allochthonous inputs on paleoclimate signals.

1. Introduction

Owing to the intrinsic complexity of the climate system, multiproxy reconstructions have become the preferred approach to assess lead-lag relationships, forcings, responses, and feedbacks. A prerequisite for any paleoclimate investigation is the establishment of a robust and precise chronostratigraphy. For marine sedimentary sequences, radiocarbon (^{14}C) dating of mono-specific planktonic foraminifera is the most employed method to establish age-depth relationships for the study of the last 50,000 yr. In turn, any proxy-records derived from the same sediment core are usually placed on the same foraminifera-based time-scale, regardless of which sediment component they are associated with. The resulting climate interpretation for a given depth horizon is thus performed under the premise that all proxies reflect water column or terrestrial conditions from the same time interval. However, prior studies have revealed variable and in some cases substantial age discrepancies among proxies within a single sediment sample (e.g. planktonic foraminifera, total organic carbon (TOC), and alkenones). For instance, age offsets of up to several millennia have been observed in the continental margins of the South China Sea, Chile, and Namibia (Mollenhauer et al., 2005), while age discrepancies are almost negligible in the Panama Basin and the NW African continental margin (Mollenhauer et al., 2005; Kusch et al., 2010). The most conspicuous case is that of Bermuda Rise drift sediments, where alkenones were found to be up to 7000 yr older than co-occurring foraminifera (Ohkouchi et al., 2002). These prior studies imply that the spatio-temporal fidelity of the derived proxy records may in some cases be compromised, hindering robust comparisons between records obtained from the same core. In reality, however, it is likely that recorded signals reflect a combination of both autochthonous and allochthonous components, giving rise to older observed ages. In the best-case scenario, contributions of old material might skew radiocarbon ages, but it would not necessarily impart an equivalent bias on the corresponding proxy

* Corresponding author.
E-mail addresses: blanca.ausin@erdw.ethz.ch (B. Ausín), c.magill@hw.ac.uk (C. Magill), negar.haghipour@erdw.ethz.ch (N. Haghipour), alvaro.bremer@erdw.ethz.ch (Á. Fernández), wacker@phys.ethz.ch (L. Wacker), dah73@cam.ac.uk (D. Hodell), baumann@uni-bremen.de (K.-H. Baumann), timothy.eglinton@erdw.ethz.ch (T.I. Eglinton).

https://doi.org/10.1016/j.epsl.2019.03.003

signal. In general, lower contributions from an allochthonous population would be expected to exert a lesser influence on the proxy signal, regardless of its impact on the ^{14}C ages. Thus, detailed assessment of possible distortions of multi-proxy records due to the addition of allochthonous/pre-aged material is warranted, particularly in cases where marine sedimentary sequences may contain information on past rapid (sub-millennial) climate and environmental changes. A case in hand are the so-called "Shackleton sites" (SW Portuguese margin), a benchmark location where climate signals related to orbital forcing, mid/high-latitude teleconnections, the bipolar ventilation seesaw, changes in the thermohaline circulation, primary productivity changes, in-phase variations with Arctic and Antarctic climate variability, and synchronicity between marine and terrestrial hydroclimate change (Hodell et al., 2013; Martrat et al., 2007; Skinner et al., 2014; Shackleton et al., 2000; Sánchez-Goñi et al., 1999) have been investigated at high temporal resolution, and using a wide range of differing proxies. Of these complementary proxies, the molecular and isotopic composition of OC has been extensively used to inform about biological productivity and organic matter (OM) preservation. The distribution and geochemical composition of source-specific organic molecules (biomarkers) such as phytoplankton-derived alkenones are used to reconstruct trends in sea surface temperature (SST) and pCO_2, while higher plant-derived long-chain fatty acids (C_{26} to C_{32} LCFAs) haven proven effective proxies of terrestrial hydroclimate. Here, we compare radiocarbon characteristics of co-occurring planktonic foraminifera, TOC, alkenones, and LCFAs in order to assess the magnitude of temporal offsets and the potential causal mechanisms in a sediment core from the Shackleton Sites. We then use this information to constrain the age structure and relative contribution of the different age pools that lead to age offsets between foraminifera versus OC and biomarkers, and evaluate the impact of down-core age discrepancies on proxy reconstructions of past climate.

2. Materials and methods

For this study, we used sediment sections from kasten core SHAK06–5K (37°34′N, 10°09′W, 2,646 m) retrieved from the "Shackleton Site" on the SW Iberian margin by RSS *James Cook* during the cruise JC089 in 2013 (Hodell et al., 2014).

2.1. Sample preparation and analytical methods

For preparation of bulk OC samples, an aliquot of 20-25 mg of freeze-dried sediment was fumigated with concentrated HCl to remove inorganic carbon and subsequently kept under basic atmosphere (pH > 7) at 60 °C. Carbon isotopic composition ($\delta^{13}C$) and TOC content of bulk OC were measured with an Elemental Analyzer (EA) interface coupled to a Mini Carbon Dating System (MICADAS). Aliquots of 20-30 mg of dry sediment were used to measure total nitrogen (N_{tot}) without previous treatment on an EA coupled in continuous-flow with an isotope ratio mass spectrometer. The total organic carbon/total nitrogen ratio (TOC/N_{tot}) was then calculated.

For biomarker analysis, a total lipid extract was obtained by microwave-extraction with $MeOH/CH_2Cl_2$ (9:1, v/v) from aliquots of freeze-dried bulk sediments (4-15 g [dry weight]), and the extract was subsequently saponified with 0.5 M KOH/MeOH. The neutral fraction, containing the alkenones and glycerol dialkyl glycerol tetraethers (GDGTs) was liquid-liquid extracted with hexane. The remaining saponified products were acidified (pH ∼ 1) prior to liquid-liquid extraction to obtain a fraction containing the LCFAs. Silica gel column chromatography was used to separate the neutral fraction into three different polarity fractions: hydrocarbons (F1), ketones and aldehydes (F2), and a polar fraction (F3), using Hexane, Hexane/CH_2Cl_2 (1:3 v/v), and CH_2Cl_2/MeOH (9:1 v/v), respectively. The F2 fraction, containing the alkenones, was analyzed by gas chromatography with flame ionization detection (GC-FID) to determine abundances and $U^{k'}_{37}$ ratios (Brassell et al., 1986). F3, containing the GDGTs, was filtered (0.45 µm pore size) and subsequently analyzed by high performance liquid chromatography (HPLC) to calculate TEX^{H}_{86} ratios (Kim et al., 2010). The latest global calibrations proposed by Tierney and Tingley (2018) and Tierney and Tingley (2015) were applied to estimate $U^{k'}_{37}$- and TEX_{86}-derived SSTs, respectively.

For compound-specific ^{14}C analyses, between 60-120 g of dry sediment was microwave-extracted and the extract was saponified as for biomarker analysis. Alkenones were isolated and purified following Ohkouchi et al. (2005). An additional silica gel (fully de-activated, 70-230 mesh) column (6 mm, i.d. ×4 cm) chromatographic separation was performed using Hexane (F1′) and Hexane: CH_2Cl_2 (2.2:1.8 v/v; F2′) to further purify the alkenones (retrieved in F2′) and remove an unknown contaminant. Approximately 40-60% of the alkenones were recovered during this step, implying partial loss of material. LCFAs contained in the acid fraction were methylated and further purified following Ohkouchi et al. (2003). Even-numbered C_{26} to C_{32} FAs were combined for ^{14}C analyses following their isolation using preparative capillary gas chromatography (PCGC), and subsequently run over short silica gel column to remove possible column-bleed contamination from degradation of the GC stationary phase. Purity and quantification of both the alkenones and LCFAs were assessed by GC-FID before direct transfer into EA tin capsules with DCM (3 × 50 µL). Samples were immediately dried on a hot plate (35 °C) to remove solvent and measured within 12 h for ^{14}C.

For isolation of planktonic foraminifera, solvent-extracted bulk sediments were wet-sieved through 300 µm and 250 µm meshes and thoroughly washed using a high-pressure stream of MilliQ® water and immediately dried (60 °C, overnight) before about 50-100 well-preserved tests of the species *Globigerina bulloides* were picked for radiocarbon dating.

Samples and associated blanks analyzed for radiocarbon were measured as CO_2 using a MICADAS equipped with a gas ion source at the Laboratory of Ion Beam Physics, ETH Zürich. Foraminifera were measured with an automated method for acid digestion of carbonates (Wacker et al., 2014; Bard et al., 2015), which enables removal of surface contaminants by the external leaching of the shells so that no further cleaning was applied after foraminifera picking. TOC, alkenones and LCFAs were measured using an online EA-AMS set up (Haghipour et al., in preperation). All reported ages for these compounds were corrected for processing blank and in the case of LCFAs, also for the addition of the derivative carbon during the methylation step using isotopic mass balance (Tables S1 and S2). For each method, ^{14}C-depleted and ^{14}C-modern standards were used. The processing blanks were prepared in the exact same way as the samples and in different sizes, as similar as possible to the target compounds. Using a constant contamination model (Hanke et al., 2017), we calculated the $F^{14}C$ and mass of extraneous carbon (mc) throughout isolation methods and applied the error propagations.

The calculated values are mc: 0.93 ± 0.19 µg with $F^{14}C$: 0.42 ± 0.02 for fatty acids. In the case of alkenones we estimated mc: 1.03 ± 0.21 µgC with $F^{14}C$ value of 0.85 ± 0.17.

2.2. Age-depth model

The age-depth model (Fig. 1A, Table S3) for core SHAK06–5K is a depositional model (P_Sequence type) developed from ^{14}C ages of monospecific samples of the planktonic foraminifera *G. bulloides* ($n = 41$) using the calibration package Oxcal (Bronk Ramsey, 2009a). Identification and exclusion of data outliers was performed

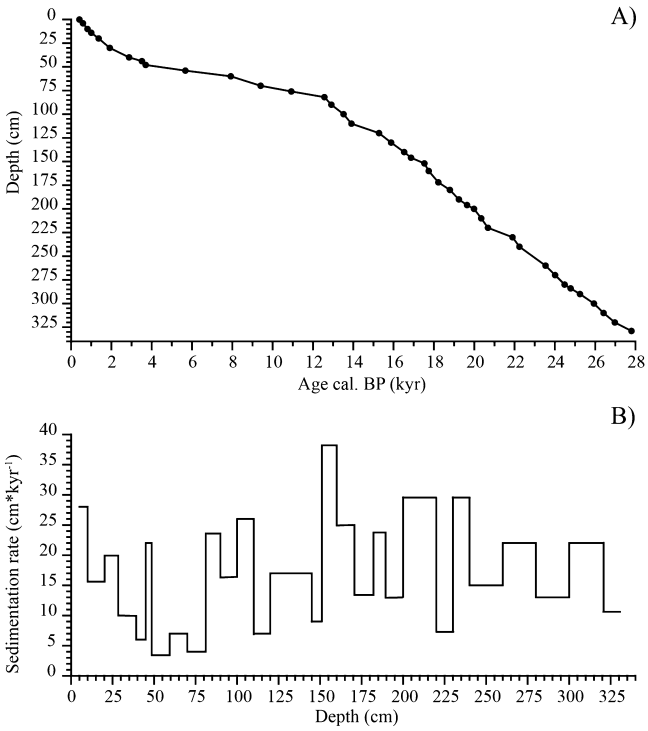

Fig. 1. Age model for core SHAK06–5K. (A) Foraminifera-based age-depth model. (B) Sedimentation rate.

according to Bronk Ramsey (2009b). Conventional radiocarbon ages (Table S1) were then calibrated to incorporate a static marine reservoir effect using Marine13 curve (Reimer et al., 2013), while no local reservoir was applied. Calibrated ages are reported at 2σ confidence level (95% probability). This age-depth model spans the last 27,000 yr, and the resulting sedimentation rate (Fig. 1B) was found to vary between 3 and 35 cm/kyr (average 16 cm/kyr).

2.3. Age structure modeling

Following the approach previously used for terrigenous biomarkers (Fornace, 2016; French et al., 2018), an isotope-mixing model was implemented to estimate ^{14}C age distributions of TOC and alkenones on the assumption that they comprise two different age populations: a decadal pool, representing freshly produced, rapidly deposited autochthonous material, and a millennial pool, representing pre-aged, allochthonous (advected) material:

$$F^{14}R = f_{dec}F^{14}R_{dec} + f_{mil}F^{14}R_{mil} \quad (1)$$

$$f_{dec} + f_{mil} = 1 \quad (2)$$

where f_{dec} and f_{mil} are the relative contribution of the decadal and the millennial pools and $F^{14}R$ is the fractional relative disequilibrium (Soulet et al., 2016) of the measured compound (Table S4), the decadal ($F^{14}R_{dec}$) and the millennial ($F^{14}R_{mil}$) pools, defined as:

$$F^{14}R = F^{14}C_{compound}/F^{14}C_{sediment}$$

$$= F^{14}C_{compound}(t_0)/F^{14}C_{sediment}(t_0) \quad (3)$$

where $F^{14}C_{compound}$ and $F^{14}C_{sediment}$ are the fraction modern of the component of interest (i.e., TOC and/or alkenones) and the sedimentary component used as reference for the deposition age in a certain depth horizon (i.e., planktonic foraminifera) (Tables S3 and S4), and t_0 is time of deposition.

The TOC and alkenones sample at 60 cm depth were excluded from the analyses given their younger-than-foraminifera ages. The model is built under the premise that the age distribution of the component of interest was constant over time. Given the large variability of the age offsets between LCFA and foraminifera, numerical simulations of the LCFA age structure was not performed. For the purposes of constraining the model, OC was assigned to be exclusively (100%) comprised of marine organic matter. This source assignment is supported by TOC/N_{tot} atomic ratios and stable isotopic data (see discussion), although it is acknowledged that terrestrial OM is present albeit in very minor proportions. Following the assumption that foraminifera, alkenones and OC were in equilibrium with surface ocean mixed layer dissolved inorganic ^{14}C at time of biosynthesis, the original $F^{14}C$ of each compound was estimated using the Marine13 calibration curve. A synthetic compound $F^{14}R$ was modeled from possible combinations of modeled $f_{dec,}$ $F^{14}R_{dec}$, f_{mil} and $F^{14}R_{mil}$. The lowest root mean squared error (RMSE) between the modeled and the measured compound $F^{14}R$ was used to determine the age structure combinations that yielded the best fit with the measured data. Further methodological details are presented in the Supplementary material.

2.4. Down-core SST modeling

We used the top 5% best fitting age distributions (lowest RSME) and their associated millennial fractions (Tables 1 and S5) to deconvolve the measured alkenone temperature record into a millennial (i.e., pre-aged allochthonous signal) and a decadal (i.e., autochthonous signal) component. The decadal component was calculated by mass balance using the millennial age structure, the fraction of millennial carbon present in the mixture, and the alkenone temperatures that were measured for the mixture.

$$SST_{dec} = (SST_{measured} - (f_{mil} * SST_{mil}))/f_{dec} \quad (4)$$

Previous evidence (Magill et al., 2018) suggests advection of pre-aged material to the core site from the western Mediterranean. Accordingly, SST_{mil} is extracted from the high-resolution alkenone-based SST record from sediment core ODP-977A in the relatively productive Alboran Sea (Martrat et al., 2004), spanning the last 245 kyr. In this way, an estimate of the autochthonous (i.e., decadal) SST was obtained for the entire length of the alkenone record for all 9575 simulated millennial age distributions.

3. Results

3.1. Radiocarbon ages

Conventional (uncalibrated) radiocarbon ages of *G. bulloides* show a constant down-core trend towards older ages, with no re-

Table 1
Top five percent best-fitting age structures with the smallest RMSE. The number of cases is 9591 for TOC and 9575 for alkenones.

	Age decadal	50% percentile age decadal	Age millennial	50% percentile age millennial	f millennial
TOC	46-86	75	27,980-49,900	40,000	0.15-0.17
Alkenones	65-86	79	18,500-49,900	34,290	0.16-0.20

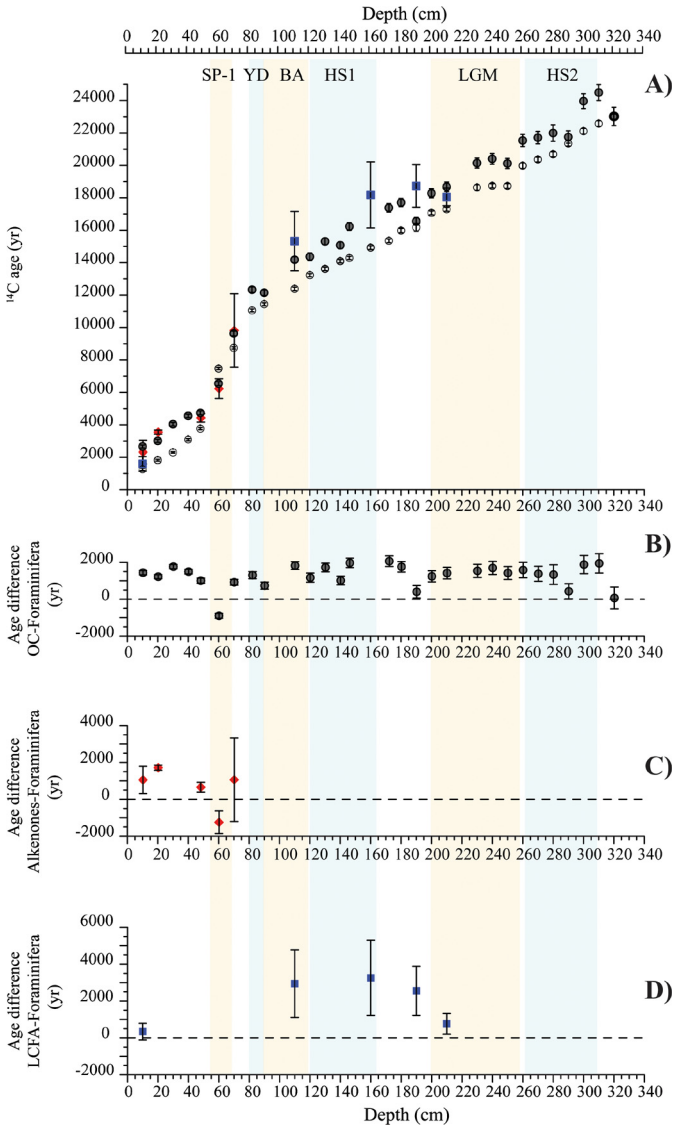

Fig. 2. Down-core radiocarbon ages of the proxy carriers and age discrepancies among them. (A) Radiocarbon ages of *G. bulloides* (open circles), OC (grey dots), alkenones (red diamonds, and long-chain fatty acids (blue squares). Error bars correspond to associated 1σ error. ^{14}C-age discrepancies between foraminifera *G. bulloides* and (B) OC, (C) alkenones, and (D) long-chain fatty acids. Error bars correspond to propagated 1σ error. (For interpretation of the colors in the figure(s), the reader is referred to the web version of this article.)

versals (Fig. 2A and Table S6). Bulk OC features a similar down-core evolution, and exhibits a consistent ^{14}C-age offset with co-existing foraminifera (median difference = 1,389 yr, $n = 29$), that falls well outside the associated 1σ analytical uncertainties (Figs. 2A and B and Table S6). One exception occurs at 60 cm, which shows considerably younger-than-foraminifera ages for OC (Table S6). Alkenone ^{14}C ages are older (falling outside the associated errors) than concurrent foraminifera for the 3 uppermost samples. They are significantly younger that foraminifera at 60 cm depth, and older but within the error at 70 cm depth (Figs. 2A and C). Age discrepancies of alkenones against their concurrent foraminifera show similar offsets as compared to corresponding OC–foraminifera ages. LCFAs are also older than paired foraminifera with associated down-core age offsets exhibiting significant variability (~350-3,250 yr) (Figs. 2A and D).

3.2. Organic matter properties

TOC content ranges from 0.5% to 0.75% and TOC/N_{tot} ratios from 4.7 and 6.2. The δ^{13}C values of bulk organic matter fluctuate around -22.5 ± 1.0‰ (Figs. 3A-C).

3.3. Sea surface temperatures

Alkenone-derived SST is ~3.5 °C warmer than GDGT-derived SST for the last glacial. This pattern reverses for the Holocene (Fig. 3D). Both SST records vary in-phase and together resolve major short-term climate changes during the last 27,000 yr (e.g., Heinrich Stadials 2 and 1 (HS2 and HS1), Bølling-Allerød (BA), and Younger Dryas (YD)). However, detailed comparison of both records reveals significant temporal offset between reconstructed temperature signals in samples deposited through the HS1 and YD with the alkenone-derived SST signal lagging that from GDGTs by 379 yr and 590 yr, respectively.

3.4. Age pool structures

A total of 191820 and 191498 possible age structure combinations were obtained from the model for TOC and alkenones, respectively (Fig. 4). Only the top five percent best-fitting age distributions and fractions based on RMSE ($n = 9591$ for TOC and $n = 9575$ for alkenones) were examined (Figs. 4, S1 and S2). TOC age structure is composed of 15-17% of millennial material of substantial age (27,980 to 49,900 yr), with the majority being decadal OC with an age of between 46 and 86 yr (Fig. 4, Table 1). Alkenone age structure correspond to a similar millennial contribution (16-20%) that exhibits a large range in age (18,500-49,900 yr), with the major contribution reflecting a decadal pool characterized by a narrower age range (65-86 yr).

3.5. SST record deconvolution

The deconvolved and the measured alkenone-derived SST records vary in phase, but the former shows higher amplitude variability and higher absolute temperatures (ave., 2.7 °C higher) than the latter (Fig. 5A). The greatest SST offset (5 °C) is observed during the Late and mid-Holocene (9-4.5 ka). For the last 16 kyr, the deconvolved SST record is more comparable to the GDGT-derived SST record (Fig. 5B), while the period from 28 to 16 ka is characterized by a constant offset of 8 °C.

4. Discussion

4.1. Pre-aged OM at the Shackleton Sites

Older-than-foraminifera ages of bulk OC indicate addition of pre-aged organic material from processes such as re-suspension/re-deposition of near bottom sediments, lateral transport (i.e., advection), and/or fluvial discharge. The magnitude of these age discrepancies (up to 2,000 yr) further indicates entrainment of predominantly allochthonous material, since local remobilization of autochthonous OM bottom sediments would have a minimal influence on radiocarbon age.

The narrow shelf that is incised by submarine canyons adjacent to the core site may serve as a source of pre-aged terrestrial OM delivered to the Iberian coastline via fluvial and/or atmospheric processes (Raymond and Bauer, 2001). However, a first-order approximation of sedimentary OM sources, based on δ^{13}C and TOC/N_{tot} atomic ratios suggests that OM accumulating at the core site is predominantly of marine origin (Figs. 3A-C), consistent with prior characterizations of OM from surface sediments in the region (Alt-Epping et al., 2007). Thus, across-shelf

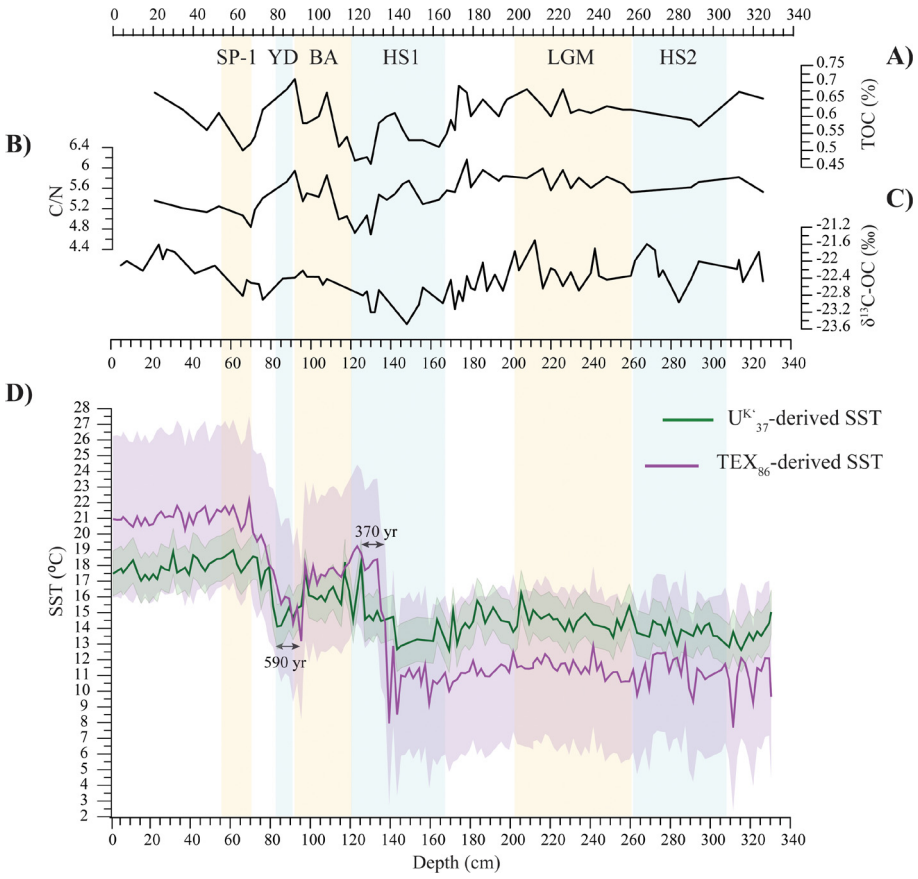

Fig. 3. Down-core stable isotopic and geochemical signatures of bulk OC and biomarker-derived SST paleorecords for core SHAK06–5K. (A) Total Organic Carbon content of bulk sediment. (B) C/N atomic ratio. (C) Carbon isotopic records. (D) Paleotemperatures derived from alkenones (green) and GDGTs (purple), and their associated 1σ uncertainty (shaded regions). Black arrows stand for temporal offsets between both records of 370 yr for the HS1 and 590 yr for the YD.

and/or along-slope transport of marine allochthonous material to the core site appears more likely as a mechanism for supply of pre-aged OC. Of these two non-exclusive mechanisms, recent evidence suggests lateral advection of mineral-hosted OC via entrainment in intermediate nepheloid layers (INLs) associated with Mediterranean Outflow Water (MOW) transport (Magill et al., 2018). The latter study found younger OC associated to the clay mineral fraction and older OC associated to fine and coarse silt fractions. The authors attributed relative changes in down-core age offsets among grain size-specific sediment OC fractions to changing hydrodynamic conditions during periods of abrupt climatic change. Although hydrodynamically-driven sorting processes are evident in measurements on specific grain sizes and can affect the fate of a significant fraction of total OC deposited during abrupt climate events, these effects do not manifest themselves in down-core sediment OC_{bulk} radiocarbon signals, the latter displaying relatively systematic age offsets relative to those of planktic foraminifera. We attribute this to signal blurring as a consequence of the predominance of pre-aged OC associated with the clay fraction (<2 μm). Indeed, fine and coarse-silt OC fractions show median age offsets of 2,178 yr and 2,431 yr, respectively, when compared to concurrent *G. bulloides* (Magill et al., 2018), whereas the median age offset for clay-associated OC is lower and relatively uniform (1,200 yr) regardless of hydrodynamic conditions, and similar to the observed OC_{bulk}-foraminifera age offsets. Clays exhibit high cohesiveness, and therefore are less susceptible to mobilization compared to slightly larger (silt) grain-size sediment fractions (Magill et al., 2018; McCave and Hall, 2006). The associated high specific surface area of the clays also supports much higher sorption of OC (Keil and Mayer, 2014), thereby increasing its proportional influence on the radiocarbon ages of OC_{bulk}. We therefore conclude that advective supply of older mineral-associated OC is the most plausible explanation for the TOC records in Shackleton Site sediments.

4.2. Age distortions affecting biomarker signals

Our results indicate alkenones are skewed towards older radiocarbon ages as compared to concurrent foraminifera throughout most of the Holocene (Figs. 1A and C). While contamination by extraneous carbon due to small sample sizes is a concern, we consider the results robust for several reasons: first, methodological and instrument blanks do not reveal any significant contamination during preparation; second, CO_2 amounts measured manometrically were comparable with those for alkenones determined by GC-FID; and third, extraneous carbon was carefully accounted for during blank correction. Moreover, coherent (i.e., in-phase) down-core variations of both alkenone and OC age offsets implies the signals are authentic and support the influence of a common transport mechanism.

As for the majority of OM in marine sediments, alkenones exhibit a strong physiochemical association with fine-grained, high-surface-area minerals (Keil and Mayer, 2014; Mayer, 1994), leading them to respond to the hydrodynamic properties of their mineral hosts. We suggest that long-distance (10-1000 km) lateral OM transport to our core site can explain the observed offsets in radiocarbon ages. This mechanism has already been invoked to explain discrepancies in alkenone and foraminifera dates in other continental margin settings (Mollenhauer et al., 2003, 2005, 2007; Kusch et al., 2010; Ohkouchi et al., 2002; Weaver et al., 1999). One exception is evident for a sample at 60 cm depth, wherein

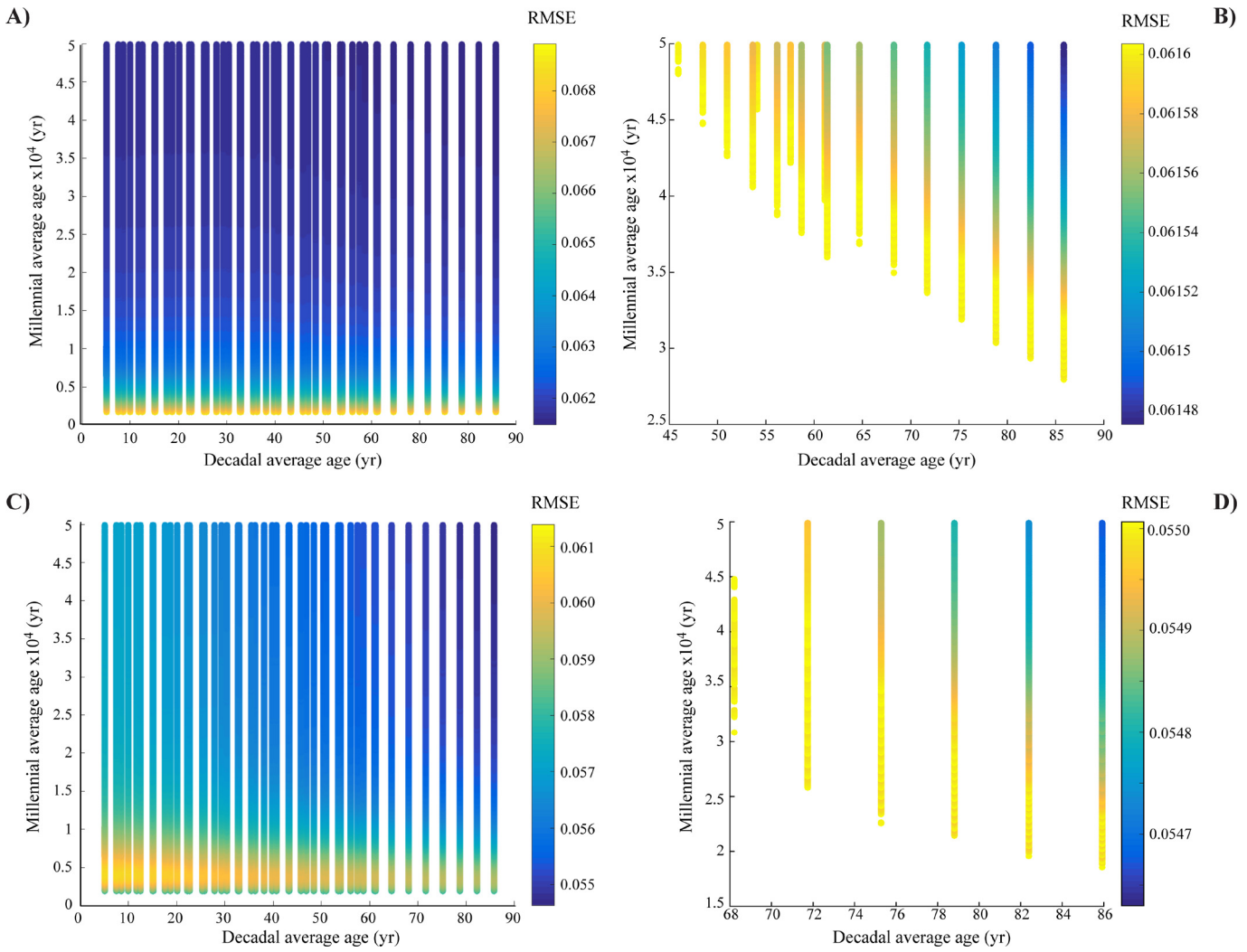

Fig. 4. Heat maps for (A and B) TOC and (C and D) alkenones, showing all the cases (left; $n = 191820$ for TOC and $n = 191498$ for alkenones) and the top five percent best-fitting age structures (right; $n = 9591$ for TOC and $n = 9575$ for alkenones). The maps represent the fit between each combination of modeled age structure and the measured $F^{14}R$ according to RMSE, where dark blue (lowest RMSE) represents the best fit.

both alkenones and OC_{bulk} are notably younger than that of corresponding foraminifera within error estimates. This sample depth correlates with an abrupt reduction in sediment accumulation rate (Fig. 1B), and falls amid the time of Sapropel 1 formation in the Mediterranean Sea (SP-1) (Mercone et al., 2000). The inferred sudden decrease of both Mediterranean outflow strength and lateral sediment supply during this period (Voelker et al., 2006) resulted in the largest decrease in sedimentation rate of this region over at least the last 30,000 yr. Deposit-feeding benthic heterotrophic fauna can introduce fine-grained organic material deeper into the sediment (Wheatcroft, 1992, and references therein), promoting younger-than-foraminifera ages for co-eval OC. Based on the model for particle-size dependent bioturbation proposed by Bard (2001), it is possible to estimate time shifts between proxy-signals respectively associated with different particle sizes. Considering a typical scenario (i.e., mixing depths of the fine and coarse fractions of 15 cm and 5 cm, respectively), and assuming a sedimentation rate of <5 cm/kyr and a climate event of 7 kyr duration, the fine fraction might be 1000-1500 yr younger than the coarse fraction. Overall, the combined effects of a significant reduction of lateral transport processes and an increase in susceptibility to particle-size induced differential bioturbation serves to explain the observed reversal in age offsets between foraminifera and organic components for this interval.

Relative radiocarbon age offsets observed between co-eval C_{26}–C_{32} FAs and foraminifera are both variable and, in some cases, large (i.e., differences of $\sim$ 350-3,250 yr) (Figs. 1A and D). Direct fluvial influences (e.g., from the Tagus River) at the SHAK06–5K site are considered minimal (Alt-Epping et al., 2009), and thus supply of pre-aged terrestrial OM (incl. LCFAs) is likely to occur via atmospheric (e.g., wind erosion, aerosol formation, rain, dry deposition, etc.) and/or oceanic (i.e., remobilization and translocation of deposited material) processes. For instance, prior studies suggest that terrestrial OM derived from distal Saharan sources influence vegetation reconstructions in marine sediments off the southwest Iberian margin (Sánchez-Goñi et al., 1999). Arid intervals associated with increased dust transport from north Africa during the YD and HS1 likewise show increased leaf-wax concentrations in regional Iberian sediments (Vegas et al., 2010). Processes associated with mobilization and aeolian dust transport (Eglinton et al., 2002) as well as across- and along-margin oceanic transport have been invoked as sources of pre-aged plant wax biomarkers (Bao et al., 2018). Thus, while specific contributions by these mechanisms with respect to LCFA deposition cannot be discerned from available data, both the magnitude of LCFA–foraminifera age offsets as well as the variability in these age offsets (100–1000s yrs) supports variable mixing of locally *vs.* remotely sourced organic matter in core SHAK06–5K. Such processes could complicate assessment of

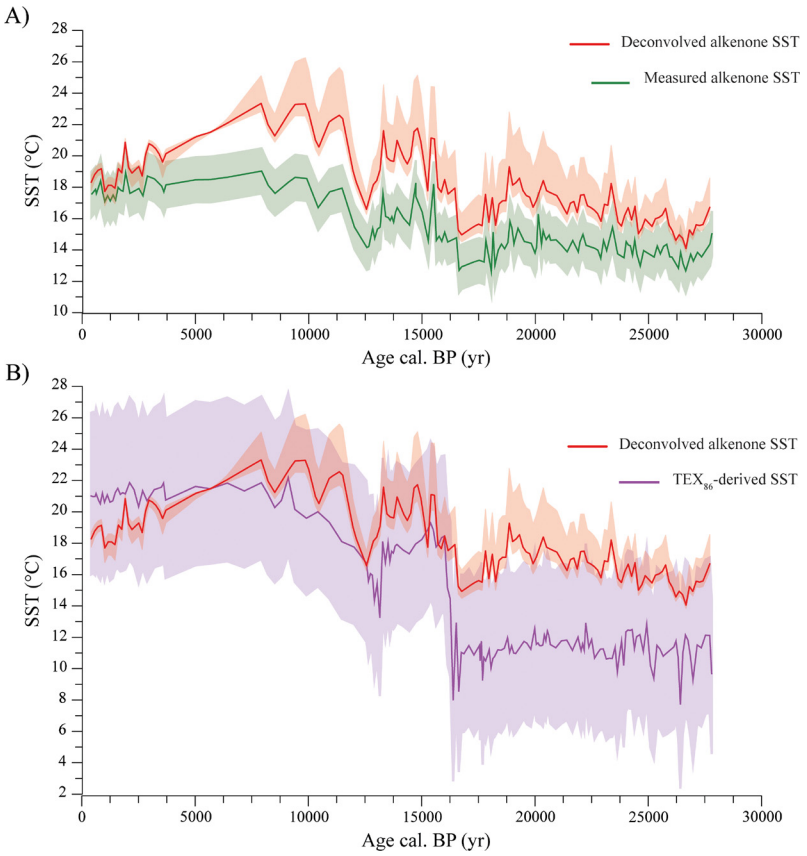

Fig. 5. Comparison of deconvolved and measured SST records from SHAK06–5K. (A) Deconvolved (red) and measured alkenones-derived (green) SST records. (B) Deconvolved (red) and measured GDGT-derived (purple) SST records. Shaded regions represent the associated 1σ uncertainty.

temporal relationships between oceanic and continental processes, and establishment of land–ocean climate connections when using proxies derived from marine and terrigenous sources.

4.3. Implications for high-resolution paleoclimate reconstructions

Proxy-specific radiocarbon dates demonstrate that temporal offsets (>1000 yr) of the derived climate signals can exceed the duration of major abrupt climate events that punctuated the last deglaciation. Thus, temporal (and also spatial) biases of the interpreted climate signal are possible. The relatively high primary productivity (and export fluxes) combined with hydrographic processes that have characterized this continental margin setting over the past (Salgueiro et al., 2010; Incarbona et al., 2010) appear to result in at least two age populations that contribute to the proxy signals. The average age of the decadal pool of both OC and alkenones (Figs. 4, S1 and S2, and Table 1) excess the duration of particle settling and points to processes such as sediment mixing via moderate bioturbation and/or re-suspension/re-deposition of near bottom sediments. The age structure of the millennial pool for both components suggests the addition of extensively pre-aged allochthonous material, having an average age that most likely exceeds that of OM aging during lateral transport. While the exact source of pre-aged TOC and alkenones remains unknown, exposure and erosion of deeper sedimentary sequences seems necessary to explain addition of substantially old marine OM. The contribution of allochthonous material is relatively minor, which diminishes the degree of proxy-record aliasing. Indeed, the excellent agreement between the timing (in-phase) of the millennial changes in planktonic $\delta^{18}O$ and $U^{K'}_{37}$ variations on the Iberian Margin during MIS 3 (Pailler and Bard, 2002) implies strong coherence in signals. Nevertheless, the magnitude of potential biases is also dependent on the extent to which the absolute value of the advected signal differs from the autochthonous one. The deconvolved down-core SST record suggests contribution of a colder allochthonous SST signal, explained by the addition of alkenones 18,500-49,900 yr older and thus biosynthesized during the glacial period. Moreover, it has be noted that the Alboran Sea was colder than the Iberian margin during the last glacial (Cacho et al., 2002). Such cold contribution promotes a general smoothing of the measured record, having a larger impact during most of the Holocene (Fig. 5). Indeed, the deconvolved record is more comparable to that derived from GDGTs for this time span (Fig. 5B). Nevertheless, temporal offsets still exist between these two records prior to the Holocene. For instance, the rise in GDGT-based SST rise towards the end of the HS1 and the SST decrease during the YD precedes that derived from alkenones. A similar temporal offset is also evident for equivalent proxy-records from nearby core MD95-2042 (Darfeuil et al., 2016), further implying differences in temporal phasing of the two proxy signals during times of rapid climate transition. It should be borne in mind that the alkenone age structure has been modeled from Holocene samples, and assumes that the calculated fraction and age structure of each pool remains constant through time. This allows deconvolving Holocene SSTs with confidence, a case that might not apply further back in time if changes in the hydrodynamic regime accompanying abrupt climate oscillations influenced the proportion and/or provenance of advected material (Magill et al., 2018). Such changes might not only explain temporal lags between the alkenones- and GDGT-derived SST records, but also their large temperature offset observed from 28 to 16 ka that the deconvolved SST records magnifies. Unfortunately, low alkenone concentrations for several depth intervals precluded determination of radiocarbon dates with sufficient accuracy to address whether age offsets were larger during abrupt climate events. Although the

specific mechanism(s) responsible for such offsets remain unclear, and factors related to alkenone and GDGT biosynthesis (e.g., nutrient availability, algal growth rates, depth and season of production) might have also played a role in paleotemperature discrepancies (Darfeuil et al., 2016), differential resistance of alkenones and GDGTs to oxic degradation during prolonged transport may be responsible (Magill et al., 2018). Inferred greater lability of GDGTs relative to alkenones may lead to predominance of more local, contemporary SST signals for the former compared to those carried by alkenones (Shah et al., 2008). Indeed, in contrast to the alkenone record, absolute values and variability of GDGT-derived SSTs in core SHAK06–5K show a strong correspondence with those of alkenone-derived SSTs from the nearby Gulf of Cadiz (Cacho et al., 2002). Therefore, (in)coherence between regional records resulting from lateral transport of fine-grained sediments is likely to be more pronounced for alkenone-based proxy signals.

5. Conclusions

Radiocarbon analyses of co-occurring planktonic foraminifera, TOC, alkenones, and LCFAs reveal temporal offsets of several thousand years among them. Such age discrepancies are attributed to the lateral supply of pre-aged allochthonous OM to the core site, suggesting that high-deposition-rate sedimentary sequences from the Shackleton Sites may be prone to spatio-temporal aliasing among proxy signals. Application of a simple age distribution model to both TOC and alkenones suggests a minor to moderate contribution of allochthonous material substantially pre-aged. Deconvolution of the measured alkenone-SST signal points to the addition of colder, allochthonous alkenones that lead to a general smoothing of the record and had the greatest impact on derived temperatures during the Late and mid-Holocene.

Author contribution

B.A., C.M. and T.I.E. planned this investigation. A.F. assisted with model implementation. N.H. and L.W. assisted with radiocarbon analyses. B.A. prepared the samples, analyzed the results and wrote the manuscript, which benefited from contributions from all the co-authors.

Acknowledgements

The authors thank Jess Adkins and two anonymous reviewers for their critical discussion to improve this manuscript. B.A. is indebted to Daniel Montluçon, who provided immeasurable expertise and guidance during the course of this research. Madalina Jaggi and the Climate Geology Group from ETHZ are acknowledged for their support in nitrogen isotope analyses. We thank Katherine L. French for her assistance during data modeling. The cores for this study were collected during Cruise 089 aboard the RSS *James Cook* that was made possible with support from the UK Natural Environmental Research Council (NERC Grant NE/J00653X/1). This study was supported by an ETH Zurich Postdoctoral Fellowship (FEL-44 15-2) from the Swiss Federal Institute of Technology in Zurich (ETHZ) and the project 200021_175823 funded by Swiss National Science Foundation.

Appendix A. Supplementary material

Supplementary material related to this article can be found online at https://doi.org/10.1016/j.epsl.2019.03.003.

References

Alt-Epping, U., Mil-Homens, M., Hebbeln, D., Abrantes, F., Schneider, R.R., 2007. Provenance of organic matter and nutrient conditions on a river- and upwelling influenced shelf: a case study from the Portuguese Margin. Mar. Geol. 243 (1), 169–179.

Alt-Epping, U., Stuut, J.-B.W., Hebbeln, D., Schneider, R., 2009. Variations in sediment provenance during the past 3000 years off the Tagus River, Portugal. Mar. Geol. 261 (1), 82–91.

Bao, R., et al., 2018. Organic carbon aging during across-shelf transport. Geophys. Res. Lett.

Bard, E., 2001. Paleoceanographic implications of the difference in deep-sea sediment mixing between large and fine particles. Paleoceanography 16 (3), 235–239.

Bard, E., et al., 2015. AixMICADAS, the accelerator mass spectrometer dedicated to C-14 recently installed in Aix-en-Provence, France. Nucl. Instrum. Methods B 361, 80–86.

Brassell, S.C., Eglinton, G., Marlowe, I.T., Pflaumann, U., Sarnthein, M., 1986. Molecular stratigraphy: a new tool for climatic assessment. Nature 320 (6058), 129–133.

Bronk Ramsey, C., 2009a. Bayesian analysis of radiocarbon dates. Radiocarbon 51 (1), 337–360.

Bronk Ramsey, C., 2009b. Dealing with outliers and offsets in radiocarbon dating. Radiocarbon 51 (3), 1023–1045.

Cacho, I., Grimalt, J.O., Canals, M., 2002. Response of the Western Mediterranean Sea to rapid climatic variability during the last 50,000 years: a molecular biomarker approach. J. Mar. Syst. 33 (34), 253–272.

Darfeuil, S., et al., 2016. Sea surface temperature reconstructions over the last 70 kyr off Portugal: biomarker data and regional modeling. Paleoceanography 31 (1), 40–65.

Eglinton, T.I., et al., 2002. Composition, age, and provenance of organic matter in NW African dust over the Atlantic Ocean. Geochem. Geophys. Geosyst. 3 (8), 1–27.

Fornace, K.L., 2016. Late Quaternary Climate Variability and Terrestrial Carbon Cycling in Tropical South America. PhD Thesis. Massachusetts Institute of Technology.

French, K.L., et al., 2018. Millennial soil retention of terrestrial organic matter deposited in the Bengal Fan. Sci. Rep. 8 (1), 11997.

Haghipour, N., et al., in preparation. Online compound specific Radiocarbon analysis (CSRA): analytical challenges.

Hanke, U.M., et al., 2017. Comprehensive radiocarbon analysis of benzene polycarboxylic acids (BPCAs) derived from pyrogenic carbon in environmental samples. Radiocarbon 59 (4), 1103–1116.

Hodell, D., et al., 2013. Response of Iberian Margin sediments to orbital and suborbital forcing over the past 420 ka. Paleoceanography 28 (1), 185–199.

Hodell, D.A., et al., 2014. The JC089 scientific party, JC089 cruise report – IODP site survey of the Shackleton sites, SW Iberian margin. British Ocean Data Centre. https://www.bodc.ac.uk/data/information_and_inventories/cruise_inventory/report/13392/.

Incarbona, A., et al., 2010. Primary productivity variability on the Atlantic Iberian Margin over the last 70,000 years: evidence from coccolithophores and fossil organic compounds. Paleoceanography 25 (2), PA2218. https://doi.org/10.1029/2008PA001709.

Keil, R.G., Mayer, L.M., 2014. Mineral matrices and organic matter. In: Treatise on Geochemistry, 2nd ed. Elsevier, pp. 337–359.

Kim, J-H., et al., 2010. New indices and calibrations derived from the distribution of crenarchaeal isoprenoid tetraether lipids: implications for past sea surface temperature reconstructions. Geochim. Cosmochim. Acta 74 (16), 4639–4654.

Kusch, S., Eglinton, T.I., Mix, A.C., Mollenhauer, G., 2010. Timescales of lateral sediment transport in the Panama Basin as revealed by radiocarbon ages of alkenones, total organic carbon and foraminifera. Earth Planet. Sci. Lett. 290 (3–4), 340–350.

Magill, C.R., et al., 2018. Transient hydrodynamic effects influence organic carbon signatures in marine sediments. Nat. Commun. 9 (1), 4690.

Martrat, B., et al., 2004. Abrupt temperature changes in the western Mediterranean over the past 250,000 years. Science 306, 1762–1765.

Martrat, B., et al., 2007. Four climate cycles of recurring deep and surface water destabilizations on the Iberian margin. Science 317, 502–507.

Mayer, L.M., 1994. Relationships between mineral surfaces and organic carbon concentrations in soils and sediments. Chem. Geol. 114 (3), 347–363.

McCave, I.N., Hall, I.R., 2006. Size sorting in marine muds: processes, pitfalls, and prospects for paleoflow-speed proxies. Geochem. Geophys. Geosyst. 7 (10).

Mercone, D., et al., 2000. Duration of S1, the most recent sapropel in the eastern Mediterranean Sea, as indicated by accelerator mass spectrometry radiocarbon and geochemical evidence. Paleoceanography 15 (3), 336–347.

Mollenhauer, G., et al., 2003. Asynchronous alkenone and foraminifera records from the Benguela Upwelling System. Geochim. Cosmochim. Acta 67, 2157–2171.

Mollenhauer, G., et al., 2005. An evaluation of ^{14}C age relationships between co-occurring foraminifera, alkenones, and total organic carbon in continental margin sediments. Paleoceanography 1, PA1016.

Mollenhauer, G., et al., 2007. Aging of marine organic matter during cross-shelf lateral transport in the Benguela upwelling system revealed by compound-specific radiocarbon dating. Geochem. Geophys. Geosyst. 8, Q09004.

Ohkouchi, N., Eglinton, T.I., Keigwin, L.D., Hayes, J.M., 2002. Spatial and temporal offsets between proxy records in a sediment drift. Science 298 (5596), 1224–1227.

Ohkouchi, N., Eglinton, T.I., Hayes, J.M., 2003. Radiocarbon dating of individual fatty acids as a tool for refining Antarctic margin sediment chronologies. Radiocarbon 45 (1), 17–24.
Ohkouchi, N., Xu, L., Reddy, C.M., Montluon, D., Elinton, T.I., 2005. Radiocarbon dating of alkenones from marine sediments: I. Isolation protocol. Radiocarbon 47, 401–412.
Pailler, D., Bard, E., 2002. High frequency palaeoceanographic changes during the past 140 000 yr recorded by the organic matter in sediments of the Iberian Margin. Palaeogeogr. Palaeoclimatol. Palaeoecol. 181 (4), 431–452.
Raymond, P.A., Bauer, J.E., 2001. Riverine export of aged terrestrial organic matter to the North Atlantic Ocean. Nature 409, 497.
Reimer, P.J., et al., 2013. IntCal13 and Marine13 radiocarbon age calibration curves 0-50,000 years cal BP. Radiocarbon 55.
Salgueiro, E., et al., 2010. Temperature and productivity changes off the western Iberian margin during the last 150 ky. Quat. Sci. Rev. 29 (5–6), 680–695.
Sánchez-Goñi, M.F., Eynaud, F., Turon, J.L., Shackleton, N.J., 1999. High resolution palynological record off the Iberian margin: direct land-sea correlation for the Last Interglacial complex. Earth Planet. Sci. Lett. 171 (123–137).
Shackleton, N.J., Hall, M.A., Vincent, E., 2000. Phase relationships between millennial-scale events 64,000–24,000 years ago. Paleoceanography 15, 565–569.
Shah, S.R., Mollenhauer, G., Ohkouchi, N., Eglinton, T.I., Pearson, A., 2008. Origins of archaeal tetraether lipids in sediments: insights from radiocarbon analysis. Geochim. Cosmochim. Acta 72 (18), 4577–4594.
Skinner, L.C., Waelbroeck, C., Scrivner, A.E., Fallon, S.J., 2014. Radiocarbon evidence for alternating northern and southern sources of ventilation of the deep Atlantic carbon pool during the last deglaciation. Proc. Natl. Acad. Sci. 111 (15), 5480–5484.
Soulet, G., Skinner, L.C., Beaupré, S.R., Galy, V., 2016. A note on reporting of reservoir ^{14}C disequilibria and age offsets. Radiocarbon 58 (1), 205–211.
Tierney, J.E., Tingley, M.P., 2015. A TEX86 surface sediment database and extended Bayesian calibration. Sci. Data 2, 150029.
Tierney, J.E., Tingley, M.P., 2018. BAYSPLINE: a new calibration for the alkenone paleothermometer. Paleoceanogr. Paleoclimatol. 33 (3), 281–301.
Vegas, J., et al., 2010. Identification of arid phases during the last 50 cal. ka BP from the Fuentillejo maar-lacustrine record (Campo de Calatrava Volcanic Field, Spain). J. Quat. Sci. 25 (7), 1051–1062.
Voelker, A.H.L., et al., 2006. Mediterranean outflow strengthening during northern hemisphere coolings: a salt source for the glacial Atlantic? Earth Planet. Sci. Lett. 245 (1–2), 39–55.
Wacker, L., Fahrni, S., Moros, M., 2014. Advanced Gas Measurements of Foraminifera: Removal and Analysis of Carbonate Surface Contamination. Ion Beam Physics. ETH Zurich Annual report: 23.
Weaver, P.P.E., et al., 1999. Combined coccolith, foraminiferal, and biomarker reconstruction of paleoceanographic conditions over the past 120 kyr in the northern North Atlantic (59°N, 23°W). Paleoceanography 14, 336–349.
Wheatcroft, R.A., 1992. Experimental tests for particle size-dependent bioturbation in the deep ocean. Limnol. Oceanogr. 37 (1), 90–104.